Neuron
Article

Sound-Driven Synaptic Inhibition in Primary Visual Cortex

Giuliano Iurilli,[1] Diego Ghezzi,[1,2] Umberto Olcese,[1,2] Glenda Lassi,[1] Cristiano Nazzaro,[1] Raffaella Tonini,[1] Valter Tucci,[1] Fabio Benfenati,[1] and Paolo Medini[1,*]
[1]Department of Neuroscience and Brain Technologies, Istituto Italiano di Tecnologia, Via Morego 30, 16163 Genova, Italy
[2]These authors contributed equally to this work
*Correspondence: paolo.medini@iit.it
DOI 10.1016/j.neuron.2011.12.026

SUMMARY

Multimodal objects and events activate many sensory cortical areas simultaneously. This is possibly reflected in reciprocal modulations of neuronal activity, even at the level of primary cortical areas. However, the synaptic character of these interareal interactions, and their impact on synaptic and behavioral sensory responses are unclear. Here, we found that activation of auditory cortex by a noise burst drove local GABAergic inhibition on supragranular pyramids of the mouse primary visual cortex, via cortico-cortical connections. This inhibition was generated by sound-driven excitation of a limited number of cells in infragranular visual cortical neurons. Consequently, visually driven synaptic and spike responses were reduced upon bimodal stimulation. Also, acoustic stimulation suppressed conditioned behavioral responses to a dim flash, an effect that was prevented by acute blockade of GABAergic transmission in visual cortex. Thus, auditory cortex activation by salient stimuli degrades potentially distracting sensory processing in visual cortex by recruiting local, translaminar, inhibitory circuits.

INTRODUCTION

In the neocortex, the barrages of synaptic input driven by ongoing neuronal activity affect neuronal responsiveness by modulating the state of the local network (Petersen et al., 2003; Tsodyks et al., 1999). The latter is indeed determined by factors such as preceding stimuli (Higley and Contreras, 2005), attention (e.g., Lakatos et al., 2008; Otazu et al., 2009), reward expectation (Shuler and Bear, 2006), motivation (Fontanini and Katz, 2006), or general changes of the behavioral state (Crochet and Petersen, 2006; Niell and Stryker, 2010). Concurrent activation of a different sensory modality is also able to modulate local, ongoing, and evoked activity in early sensory cortices (Bizley et al., 2007; Ghazanfar et al., 2005; Kayser et al., 2008; Lakatos et al., 2007).

Cross-modal modulatory effects, assessed by extracellular recordings, are thought to consist of subthreshold responses, because suprathreshold, cross-modal sensory responses are rare in primary areas, albeit previous reports showed relatively high percentages of multimodal spiking responses in cat primary visual cortex V1 (Fishman and Michael, 1973; Morrell, 1972). Together, these findings challenge the idea that mammalian primary sensory cortices are strictly unisensory (Driver and Noesselt, 2008; Stein and Stanford, 2008).

Recent field potential recordings indicate that hetero-modal influences on primary sensory cortices cause phase resetting of local network fluctuations, mostly in supragranular layers (Kayser et al., 2008; Lakatos et al., 2007). Although the sign of heteromodal modulation of neuronal responsiveness (enhancement versus suppression) depends on the relative timing (Kayser et al., 2008; Lakatos et al., 2007) of the two stimuli, in most cases the effect on neuronal firing is suppressive. This suppression is reminiscent of the cross-modal GABA-dependent inhibition observed in associative cortices of cat (Dehner et al., 2004). Taken together, these observations raise the intriguing possibility that the recruitment of GABAergic networks could play an important role in inter-areal communication, even at the level of early sensory areas.

However, the synaptic character of hetero-modal inputs to microcircuits in primary sensory cortices, as well as their impact on responsiveness to stimuli of the dominant modality remain elusive. To address this issue, we measured the synaptic responses of pyramidal neurons in V1 upon stimulation of non-dominant (auditory and somatosensory) modalities, using in vivo whole-cell recordings guided by intrinsic signal imaging. We found that activation of auditory cortex by a brief noise stimulus recruits inhibitory circuits in V1 originating from deep, infragranular layers of V1. This acoustic-driven inhibition reduces visual synaptic and spike responses in overlying, supragranular layers of V1. We finally examined the behavioral relevance of sound-driven inhibition in V1.

RESULTS

Sound Hyperpolarizes L2/3Ps of V1

We first measured auditory responses in V1 by recording field potentials (FP) in lightly anaesthetized and awake mice (for monitoring anesthesia level, see Supplemental Experimental Procedures and Figure S1 available online). A noise burst (50 ms; 72 dB SPL) elicited a positive-going FP response in V1 of both lightly anaesthetized and awake mice (Figure 1A). Auditory-driven responses were barely visible on single trials and emerged only in the averaged trace (Figure 1B, left), in line with the

observation that heteromodal stimuli reset the phase of ongoing oscillations, without changing FP amplitude (Kayser et al., 2008; Lakatos et al., 2007). Consistently, the power of low-frequency (0–30 Hz) oscillations increased in the average response within 250 ms (Figure 1B, right). This was barely observed in single trials (Figure 1C, left). Thus, the averaged FP response emerges from a sound-driven alignment of the phase of low-frequency oscillations, as confirmed by a sound-driven increase in the inter-trial coherence of V1 FP (0–30 Hz; Figure 1C, right).

The phase resetting of ongoing oscillations is a manifestation of inter-modal modulation of the excitability of a primary sensory cortex. To investigate the underlying subthreshold events, we paired supragranular FP recordings with in vivo whole-cell current-clamp recordings from layer 2/3 pyramidal neurons (L2/3Ps). The upward FP responses were accompanied by hyperpolarizing membrane potential (V_m) responses in all cells (Figures 1D and 1E; n = 19 cells from 12 mice; amplitude: −3.5 ± 0.3 mV). Sound-driven hyperpolarizations (SHs) were also present in awake, head-fixed mice (Figure 1E; n = 3 cells from 3 mice). The hyperpolarizations were not preceded by depolarizations and sometimes were followed by a depolarizing plateau (9 out of 19 cells). SHs had an onset latency of 35.8 ± 2.2 ms, a peak latency of 134.9 ± 9.7 ms, and a median half-width of 218.1 ms.

We next tested the effects of different sound intensities on the amplitude of both FP and V_m responses (n = 17 from 8 mice; Figure 1F). A noise burst of 48 dB SPL caused a small hyperpolarization (−1.6 ± 0.2 mV), which was just above the limit of detection (defined as baseline ± 2 SD; gray bar in Figure 1F). This response became about 2-fold larger for 56 dB SPL stimuli (2.8 ± 0.3 mV) and saturated at intensities higher than 64 dB SPL (SHs > 3 mV; $p > 0.1$ for post-hoc test). Thus SHs in L2/3Ps of V1 are graded for lower intensities but steeply reach a saturating plateau. All our subsequent experiments were done with a sound intensity evoking a saturating response (72 dB SPL).

Sound-Driven Hyperpolarizations in V1 Require Activation of Auditory Cortex and Are Relayed via Cortico-cortical Connections

We next investigated whether activation of primary auditory cortex (A1) is required for SHs in V1. First, we tested whether optogenetic activation of A1 with a 2 ms pulse of blue light in Thy1::ChR2 mice, which express channelrhodopsin mostly in layer 5 (Gradinaru et al., 2009), can mimic the effects of a noise burst in V1. A1 photostimulation evoked hyperpolarizing responses in V1 L2/3Ps (Figures 2A and 2B; n = 8 cells from 6 mice; average amplitude = −4.8 ± 0.8 mV).

The onset latency of A1 photostimulation-driven hyperpolarizations in V1 L2/3Ps was 24.8 ± 1.3 ms. Given that auditory spiking responses in A1 have an onset latency of ~11 ms (Sakata and Harris, 2009), our data are consistent with A1 driving SHs in V1 (SHs onset in V1 was 35.8 ± 2.2 ms).

Hyperpolarizations of L2/3Ps in V1 driven by photostimulation could reflect a more widespread cross-areal inhibition phenomenon, rather than being unique or restricted to A1. Indeed, photostimulation of somatosensory (barrel) or associative (lateral V2) cortices also caused hyperpolarizing responses in L2/3Ps V1 (Figure S2A; barrel cortex: n = 8 cells; amplitude: −5.1 ± 0.9 mV; lateral V2: n = 6 cells; amplitude: −5.6 ± 0.8 mV). Thus, cross-areal inhibition may be a general phenomenon in neocortex.

Since photostimulation experiments do not conclusively prove the presence of an auditory input from A1 to V1, we performed a causal experiment by recording sound-driven responses in V1 L2/3Ps while silencing A1 with muscimol (Figure 2C). A1 inactivation largely abolished SHs in V1 (Figure 2D; n = 18 cells in 9 mice; amplitudes: −1.2 ± 0.3 versus −3.5 ± 0.3 - red and black, respectively; $p < 0.001$ for post hoc test). We monitored the time course of the recovery of A1 responsiveness after muscimol application (6 mice; Figure S2B). We found that the acoustically evoked FP (AEP) in A1 recovered after 5 hr from muscimol application in A1. At that time point, SHs in L2/3Ps in V1 also recovered to control levels (Figure 2D, blue; n = 11; −3.7 ± 0.6 mV after recovery, $p = 0.7$ for Tukey post hoc test). Overall, these data are consistent with A1 activation being causal to sound-driven hyperpolarizations in V1.

We next investigated the anatomical pathway by which A1 produces SHs in V1. As cortico-cortical connections from A1 to visual cortices have been described in rodents (Campi et al., 2010; Laramée et al., 2011; Paperna and Malach, 1991), we decided to investigate whether SHs in V1 L2/3Ps are relayed from A1 via cortico-cortical connections. To this aim, we performed transections between A1 and V1 guided by intrinsic signal imaging (Figure 2E). We took care that the transection reached the white matter in all sections as cortico-cortical fibers also pass through the white matter (DeFelipe et al., 1986; Figure 2E). Moreover, the amplitude and latency of visually evoked potentials (VEPs) and AEPs measured in V1 and A1 before and after the cut were unaffected by the transection (Figure 2F; grand-averages in black and red, respectively; peak amplitudes: 432 ± 43 versus 389 ± 66 μV in A1, 139 ± 44 versus 127 ± 23 μV in V1; peak latencies: 32 ± 13 versus 32 ± 14 ms in A1, 207 ± 47 versus 214 ± 36 ms in V1; $p > 0.4$). These results indicated that we did not severe the driving thalamocortical projections. However, transecting cortico-cortical connections between A1 and V1 abolished sound-driven hyperpolarizations in V1 L2/3Ps (Figure 2G; n = 14 cells from 6 mice; −3.3 ± 0.3 mV versus −0.1 ± 0.3 mV; $p < 0.001$).

Heteromodal Hyperpolarizations Are Widespread among Primary Sensory Cortices

We next wondered whether hetero-modal hyperpolarizations occur only in V1 in response to acoustic stimuli or whether they are also present in other primary cortices. To this end, we used intrinsic imaging to guide in vivo whole-cell recordings of L2/3Ps in A1 and in a barrel-related column in the primary somatosensory cortex (S1), as well as in V1. We asked whether L2/3Ps in each area were affected by sensory stimulation of the other two nondominant modalities (Figure 3). Noise bursts caused hyperpolarizations also in S1 (n = 6 cells from 3 mice; amplitude: 5.2 ± 0.3 mV; onset latency 31.3 ± 2.2 ms; peak latency 109.1 ± 9.4 ms). Similarly, multiwhisker back deflections elicited hyperpolarizations in V1 (n = 6 cells from 3 mice; amplitude: −1.5 ± 0.6 mV; onset latency 45.9 ± 4.9 ms; peak latency

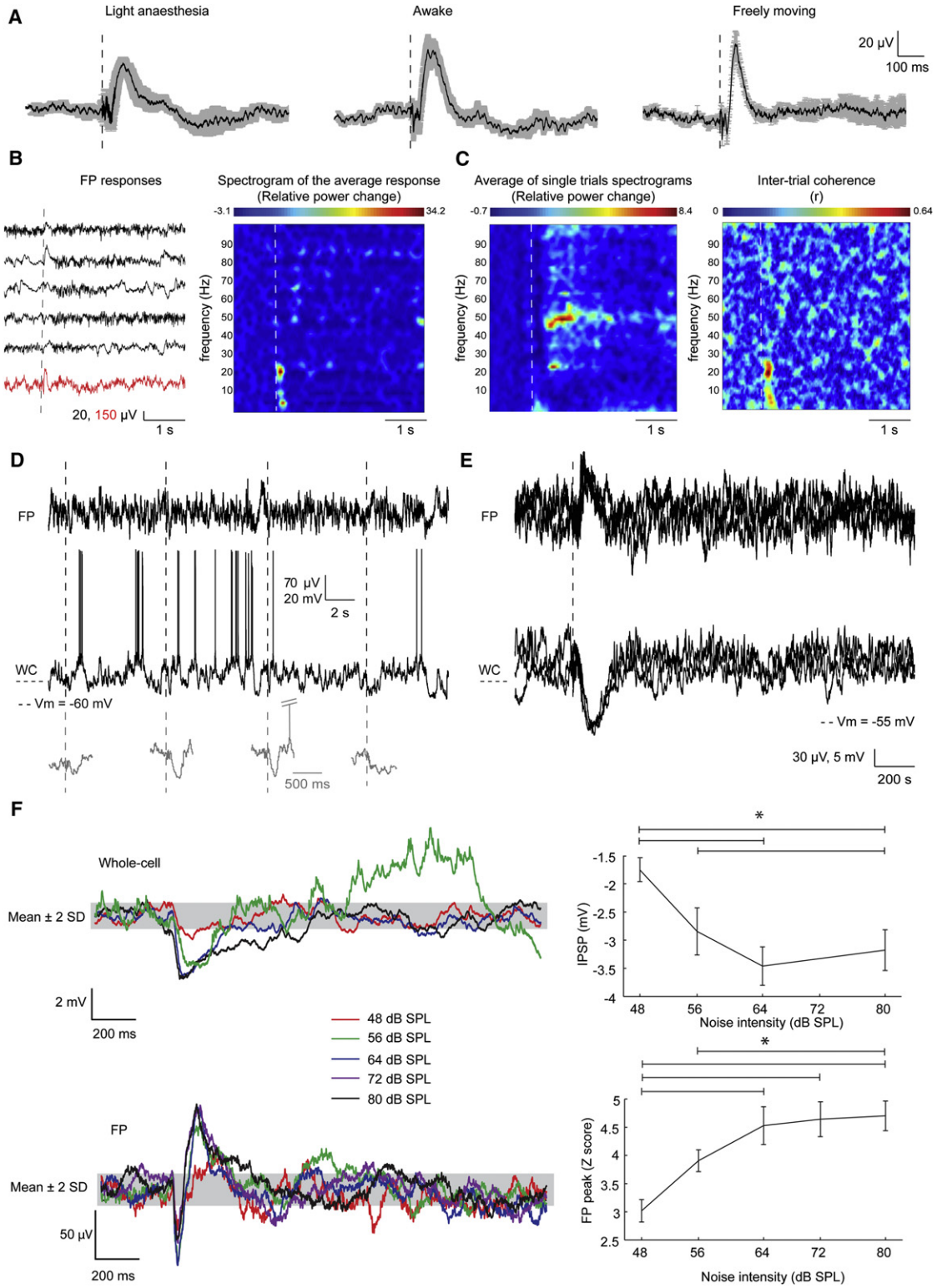

Figure 1. Sound Causes Upward FP Deflections in V1 that Are Accompanied by Cellular Hyperpolarizations

(A) The grand average ± SEM of FP responses recorded in lightly anesthetized (n = 12) and awake, head-restrained (n = 3), and freely moving (n = 6) mice. Dashed lines are stimulus onsets.

(B) Left: examples of individual FP recordings (black) aligned with the onset of a noise burst, averaged over 50 presentations (red). Right: change of spectral content over time relative to the baseline (1 s) of the averaged FP response.

172.0 ± 19.4 ms) and A1 (n = 6 cells from 3 mice; amplitude −2.2 ± 0.3 mV; onset latency 44.3 ± 5.9 ms; peak latency 156.4 ± 14.5 ms). We exclude that piezo-driven hyperpolarizations in V1 and A1 were due to an inadvertent activation of A1 and V1, respectively, by the piezo movement since mice's ears and eyes were kept closed during multiwhisker stimulation. Further, we did two control experiments to confirm that *in these conditions* hyperpolarizations in V1 and A1 were merely due to somatosensory stimulation. First, piezo activation (touching the whiskers) did not evoke excitatory responses in A1, indicating that whisker-driven hyperpolarizations in V1 were not SHs due to A1 activation by the piezo vibrations. Second, piezo movement in absence of contact with the whisker tips failed to evoke detectable responses in both A1 and V1 (Figure S3A).

The data indicate that acoustic and somatosensory stimulations caused widespread and near synchronous hyperpolarizing responses in nonauditory or nonsomatosensory primary areas, respectively. Transient visual stimulation had different effects on S1 and A1 neurons. Light spots flashed in the central binocular field caused small depolarizing responses in the majority of S1 L2/3Ps (11/13 cells from 7 mice; amplitude 3.6 ± 0.5 mV; onset latency 128.2 ± 17.2 ms; peak latency 288.0 ± 21.2 ms). This visual effect in S1 was only subthreshold, as it did not drive the cells to fire (Figures S3B and S3C). On the other side, visual stimulation with either flashes and or patterned stimulation (gratings) failed to evoke detectable subthreshold responses in A1 L2/3Ps (n = 14 cells in 8 mice).

Role of GABA in Sound-Driven Hyperpolarizations

To clarify the synaptic character of heteromodal hyperpolarizations, we focused on SHs in area V1 and investigated whether local GABAergic synapses of V1 are responsible. Using current injection, we found a decrease of membrane resistance during SHs, consistent with a role of GABA (Supplemental Experimental Procedures; Figure 4A, middle; n = 5 cells from 3 mice; −30.3% ± 7.1% compared to baseline). The decomposition of the sound-driven increase in membrane conductance into excitatory and inhibitory components indicated that noise bursts elicited the opening of inhibitory conductances (5.7 ± 1.1 nS), associated with a smaller withdrawal of excitation (−0.4 ± 0.2 nS; Figures S2C–S2E). A similar pattern of inhibitory and excitatory conductance changes was evoked by photostimulation of A1 (Figure 2B).

We next directly tested the effects of GABA blockade on SHs. First, we blocked $GABA_A$ and $GABA_B$ receptor-mediated inhibition by intracellularly perfusing neurons with picrotoxin (PTX) and cesium (Cs) ion. Great care was taken to minimize picrotoxin spillover, monitoring concurrent extracellular activity (Figure S4A). To check whether this manipulation was effective in blocking GABAergic inputs onto L2/3 s of V1, we examined the intracellular responses to local electrical stimulation (see Supplemental Experimental Procedures), which has been shown to evoke robust inhibitory responses (Contreras et al., 1997; Douglas and Martin, 1991). We found that intracellular PTX/Cs abolished the large hyperpolarizing responses observed upon microstimulation (Figure S4B; n = 11 from 5 mice; −11.4 ± 0.8 versus −1.5 ± 0.4 mV before and after intracellular perfusion, respectively, $p < 0.001$). SHs also vanished in most cells during intracellular perfusion with PTX/Cs (Figure 4B; n = 17 cells from 9 mice; −3.5 ± 0.3 versus −1.3 ± 0.4 mV, $p < 0.01$). Simultaneously recorded FP responses remained unchanged, however, indicating that the intracellular perfusion did not prevent SHs in neighboring cells (Figure S4C).

Second, we blocked $GABA_A$ or $GABA_B$ receptors by topical application of gabazine or CGP52432, at concentrations that did not cause epileptiform activity (1.5 μM and 1 μM, respectively; Figure S4D–S4F). We recorded 8 cells under gabazine, 15 cells under CGP52432 and 6 cells under a cocktail of both drugs. These experiments showed that SHs are composed of an early, $GABA_A$-IPSP and a late, $GABA_B$-IPSP (Figure 4C). Gabazine left only a late component of SHs (Figure 4D, right plot; median onset latency: 161.5 ms), while blocking their early phase (Figure 4C, top; postsynaptic potential [PSP] peaks within 0–150 ms poststimulus: −3.4 ± 0.4 versus 1.4 ± 0.7 mV, $p < 0.001$ for post hoc test). Gabazine (either alone or in combination with CGP52432) unmasked a small excitatory response, indicating that acoustic stimulation also activates some excitatory synapses whose effects are masked by inhibition (6 out of 14 cells). CGP52432 reduced the late SH (Figure 4C, bottom plot; PSP peaks within 150–400 ms poststimulus: −2.5 ± 0.2 versus −1.1 ± 0.4 mV, $p < 0.01$ for post hoc test), thus shortening SHs (Figure 4E; median half-widths: 85.4 ± 8.0 versus 227.2 ± 19.5 ms in controls, $p < 0.001$ for post hoc test). Concurrent $GABA_A$ and $GABA_B$ antagonists application counteracted SHs (−3.5 ± 0.3 versus 1.0 ± 1.3 mV, $p < 0.01$ for post hoc test) during both the early and late phases of SHs (Figure 4C, blue). Overall, these data indicate that SHs in V1 are due to the recruitment of GABAergic synapses.

Sound-Driven Activation of an Interlaminar Inhibitory Circuit in V1

We next characterized the sub- and suprathreshold effects of noise bursts across the other layers of V1: layer 4 pyramids (L4Ps; n = 5), layer 5 pyramids (L5Ps; n = 12), and layer 6 pyramids (L6Ps; n = 7). Examples of biocytin-filled cells are shown in Figure S5A. Noise bursts elicited SHs in all recorded L6Ps, whereas they failed to elicit detectable responses in L4Ps (Figure 5A). Responses of L5Ps were heterogeneous: of 12 L5Ps,

(C) Same plot as in B for individual trials (left) and intertrial coherence, measured as the phase-locking factor between trials (right). Note the prominent gamma band after the SH.
(D) Examples of simultaneous FP and whole cell (WC) recordings of the V_m from a L2/3P in V1. Magnified SHs are depicted in gray.
(E) Overlaid FP and V_m responses of a L2/3P in an awake mouse. Upward FP responses reflect hyperpolarizations.
(F) Intensity response of SHs. Examples of V_m (top) and FP (bottom) responses for different sound intensities. The response was barely detectable for 48 dB SPL sound intensity and quickly reached a saturating plateau for sound intensities > 64 dB SPL (*$p < 0.05$ for post hoc tests). Error bars in right plot are SEMs. The gray band depicts the detection level (>baseline ± 2 SD).
See also Figure S1.

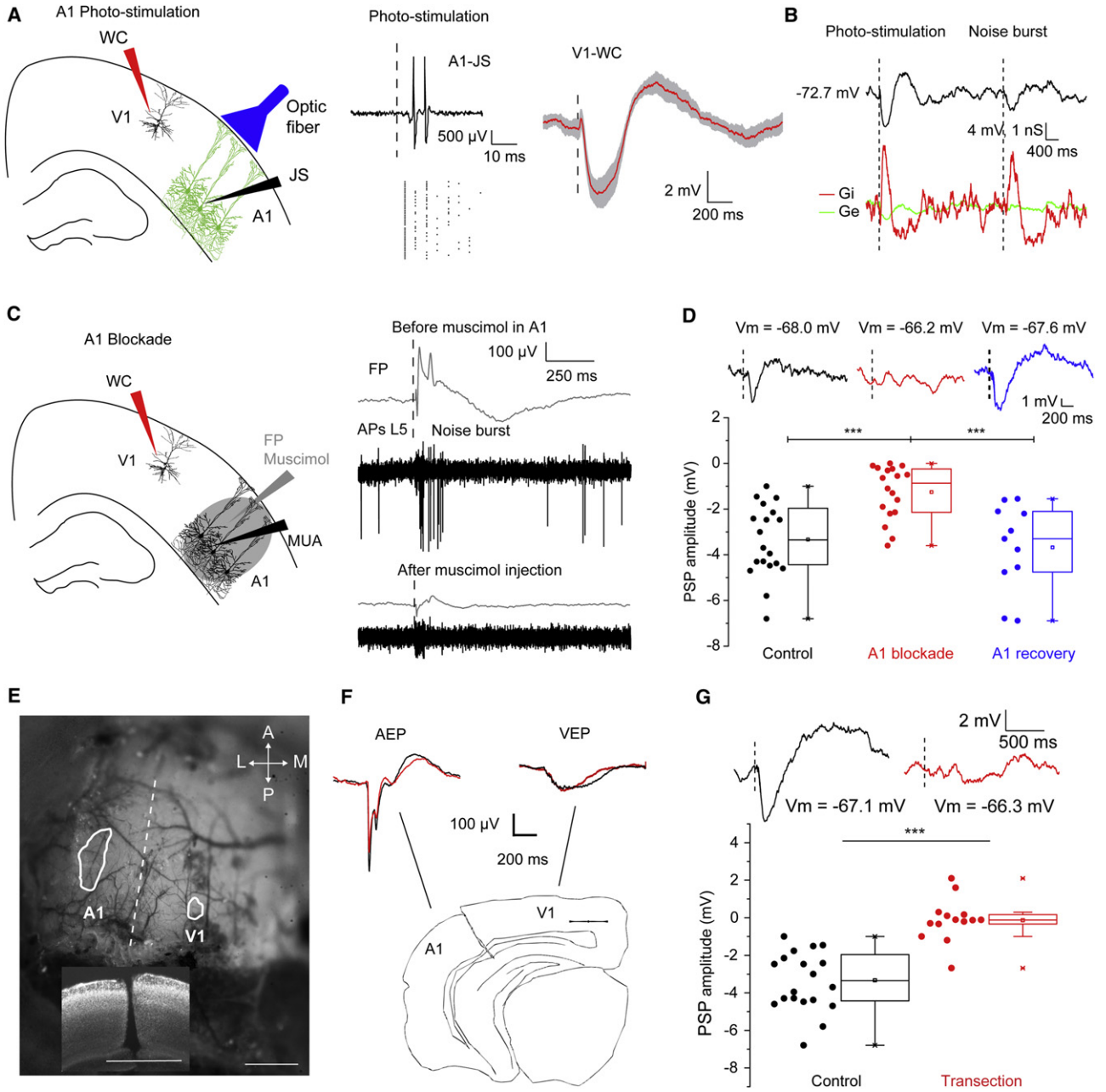

Figure 2. A1 Activation Causes SHs in L2/3Ps of V1

(A) Left: suprathreshold responses were recorded in layer 5 of A1 in juxtasomal configuration (JS) and V_m responses of L2/3Ps were measured in V1 upon A1 photostimulation. Middle: A1 photostimulation caused spiking of A1 L5Ps, as assessed by JS recordings. Right: A1 photostimulation caused hyperpolarizing responses in L2/3Ps of V1 (n = 8; grand average ± SEM).

(B) Example of hyperpolarization of a V1 L2/3P evoked by photostimulation of A1 and by sound in a Thy1::ChR2-EYFP mouse (black). Both evoked a comparable pattern of excitatory (Ge, green) and inhibitory (Gi, red) conductance changes.

(C) Muscimol in A1 silenced acoustically-evoked FP (gray) and spiking (black; MUA: multiunit activity) responses measured in the layer 5 of A1.

(D) Top: representative sound-driven V_m responses in V1 in controls (black), after A1 inactivation (red) and after the functional recovery of A1 (blue). Bottom: corresponding box plots (***$p < 0.001$ for Tukey post hoc tests).

(E) Sketch of an ISI-targeted transection between V1 and A1. The bottom inset shows the coronal level and that the depth of the transection in Nissl-stained sections reached the white matter. Bars, 1 mm.

(F) Drawing of a cortical transection across a coronal slice. The transection did not affect VEP and AEP response in V1 and A1, respectively (n = 6; grand averages; black traces: before the transections, red: after the transections).

(G) Examples (top) and box plots (bottom) showing that A1-V1 transection abolished SHs in L2/3Ps of V1 (***$p < 0.001$). Dashed lines are stimulus onsets. See also Figure S2.

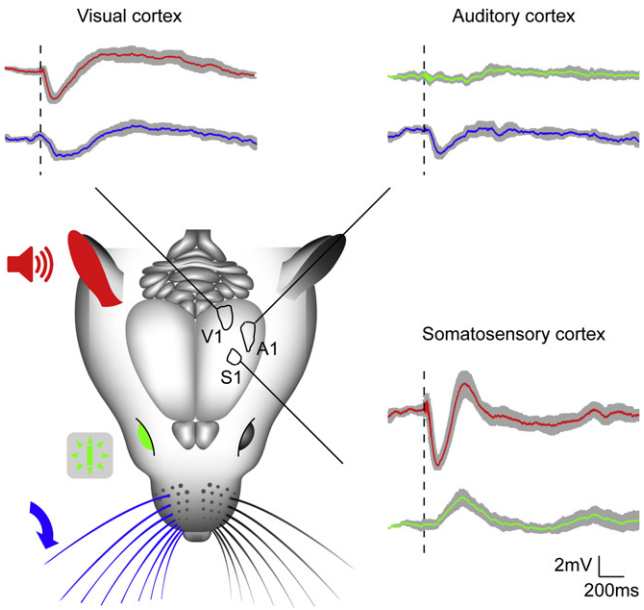

Figure 3. Heteromodal Hyperpolarizations Are Widespread among Primary Sensory Cortices

Auditory stimulation (red) caused hyperpolarizations in V1 and S1 (n = 19 and n = 6, respectively). Multiwhisker deflections (blue) caused hyperpolarizations in V1 and A1 (n = 6 for both groups). Visual stimulation (green), failed to evoke detectable responses in A1 (n = 14), but depolarized S1 L2/3Ps (n = 13). Grand averages ± SEM are shown. Dashed lines are stimulus onsets. See also Figures S2 and S3.

4 were hyperpolarized, 3 were depolarized, and 5 were unaffected by sound presentation. Extracellular tetrode recordings, which have a higher sampling capability compared with in vivo whole-cell recordings, confirmed the presence of sound-driven spiking units in infragranular layers of V1 (see examples of simultaneously recorded units in Figure 5B). Out of 34 isolated units in infragranular layers, 8 increased firing in response to acoustic stimulation, 12 decreased firing, and 14 showed no effect on ongoing firing. Interestingly, the auditory-driven firing of these infragranular units either preceded (4/8) or accompanied the SH of L2/3Ps (Figure S5B). Thus, we asked whether infragranular neurons could trigger sound-driven IPSPs in L2/3Ps of V1.

To investigate whether L5Ps activation causes hyperpolarizing responses in L2/3Ps within the same functional column, we took advantage of the fact that in Thy1::ChR2-EYFP mice, expression of ChR2 is largely restricted to L5Ps. A 2 ms light pulse in V1 was able to cause hyperpolarizing responses in all patched L2/3Ps, and the hyperpolarizations were larger (−8.7 ± 1.3 mV) and occurred earlier (onset latency: 18.2 ± 2.4 ms) compared to SHs (n = 5 cells from 4 mice; Figure 6A). Notably, this delay corresponds to the difference between the onset latency of SHs in L2/3Ps and that of sound-driven *activation* of L5Ps in V1 (Figure 6B).

More importantly, we tested the role of layer 5 in SHs of L2/3Ps by silencing activity in infragranular layers of V1 with a local puff of muscimol. We also used the injecting pipette to record multiunit activity in layer 5 (Figure 6C). We found that the multiunit activity was silenced, confirming the neuronal inhibition (Figure 6D, gray). We then patched the overlying L2/3Ps (Figure 6D, black) to look for physiological evidence for muscimol leakage into the supragranular layers. The average V_m of the L2/3Ps was not significantly different from that recorded without muscimol injected into the deep layers (Figure 6D, left plot). We also found no change in V_m *variance* in L2/3Ps after muscimol injection into the deep layers, suggesting that muscimol did not leak into the supragranular layers and affect the dynamics of spontaneous activity (Figure 6D, right plot). Indeed, V_m were dramatically more hyperpolarized and their variance reduced in case of muscimol diffusion indicating an effective shunting of ongoing activity (labeled as "Cortex" in the plots of Figure 6D; n = 7). In a subset of experiments (n = 8), we used red-fluorescent muscimol to monitor the extent of muscimol diffusion. Postmortem, in all cases we found that muscimol diffusion remained restricted to the infragranular layers (6 mice, see Figure 6C and the fluorescence intensity profiles along the depth of the cortex in Figure S6). These combined data argue that there were no direct effects of muscimol in the supragranular layers after deeplayer injection, and thus that we were able to selectively inhibit the infragranular layers.

Infragranular layer blockade with both normal and fluorescent muscimol abolished SHs in overlying L2/3Ps (Figure 6E; n = 16, 14 mice; −3.5 ± 0.3 versus 0.3 ± 0.7 mV, $p < 0.001$; data from animals injected with normal and fluorescent muscimol were cumulated as they were statistically undistinguishable: 0.3 ± 1.2 versus 0.4 ± 0.8 mV; $p = 0.9$). Thus, both local GABA blockade and silencing of layer 5 effectively counteracted SHs in V1 L2/3Ps. Overall, the data argue that translaminar (infragranular to supragranular) inhibition is important for the generation of SHs in L2/3Ps of V1.

Effects of Sound-Driven Hyperpolarizations on Electrophysiological and Behavioral Visual Responsiveness

What is the impact of sound-driven IPSPs on sub- and suprathreshold visual responses of V1 neurons? Based on the observed latency of SHs, we presented the noise burst so that the SH peak would coincide with the peak of the synaptic visual response evoked by optimally oriented moving bars (Figure 7A). Combining the auditory and visual stimulation in this way significantly reduced the amplitude of visually driven depolarizations (Figure 7B; n = 9, 5 mice; 14.4 ± 1.8 versus 9.7 ± 1.7 mV, $p < 0.001$). Combined auditory and visual stimulation also reduced action potential (AP) responses compared to pure visual stimulation, in terms of both peak and total number of spikes per stimulus (Figure 7B; medians: 6.6 versus 1.2 Hz and 0.48 versus 0.05 APs, respectively; $p < 0.05$). Moreover, bimodal stimulation reduced the reliability of visually driven spiking, as indicated by an increase of the coefficient of variation for APs counts on single trials (Figure 7B; medians: 1.74 versus 2.71, $p < 0.05$).

Based on these results, one could expect that a noise burst would degrade visual perception. We tested this prediction by comparing the behavioral response to a simple visual stimulus presented alone or with a simultaneous noise burst (Figure 8A). Mice were first conditioned by pairing the visual stimulus (50 ms flash, 25% luminance change) with an electric foot-shock occurring 250 ms later. This caused the emergence of a visually driven conditioned motor response (V-CMR). V-CMR was expressed as the normalized peak of locomotor activity, measured

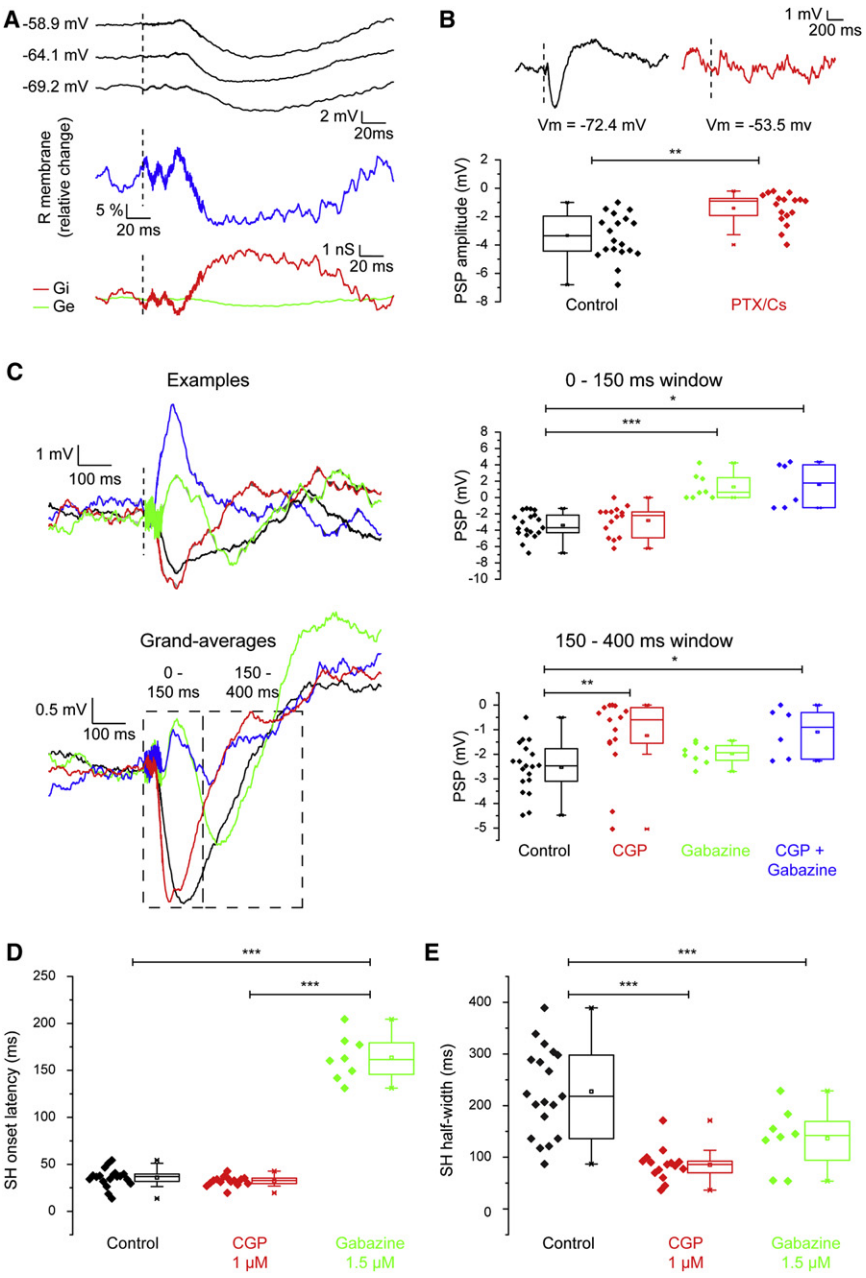

Figure 4. GABAergic Inhibition Is Responsible for SHs in L2/3Ps of V1

(A) Changes in excitatory (Ge, green) and inhibitory (Gi, red) conductances evoked by sound in a V1 L2/3P. Top: V_m responses under different current injections (from top: 100 pA, 0 pA, −100 pA). Middle: note the decrease of membrane resistance (R) during the SH. Bottom: time courses of the changes of G_e and G_i.

(B) Examples and box plots of subthreshold acoustic responses in controls (black) and during intracellular perfusion with 1 mM PTX/Cs (red). This manipulation significantly counteracted SHs (**$p < 0.01$).

(C) Examples, grand-averages (left) and amplitudes (right plots) of subthreshold responses to sound measured within 150 ms (top plot) and between 150 and 400 ms (bottom plot) poststimulus in the presence of $GABA_A$ (gabazine 1.5 µM, green, n = 8), $GABA_B$ (CGP52432 1 µM, red; n = 15) antagonists or both (blue; n = 6). Gabazine and CGP52432 effectively counteracted SHs in the early (***$p < 0.001$, for post hoc test) and late (**$p < 0.01$, for post hoc test) time windows, respectively.

(D and E) Effects of $GABA_A$ and $GABA_B$ antagonists on SH kinetics. Onset latencies (D) and half-widths (E) of SHs under $GABA_A$ (green) or $GABA_B$ (red) antagonists. (D) Gabazine significantly delayed the onset of SHs (***$p < 0.001$, for post hoc test). (E) Both gabazine and CGP52432 significantly shortened SHs (***$p < 0.001$, for post hoc test).

See also Figure S4.

around the expected time of the electrical shock (200–400 ms, see Supplemental Experimental Procedures). This V-CMR required the integrity of V1, because acute, bilateral intracortical infusions of muscimol in V1 during conditioning prevented the acquisition of V-CMRs (Figure 8B; 8 controls versus 3 muscimol-injected mice, $p < 0.05$). We next examined the effects of sound on V-CMRs by pairing flashes and sounds at various stimulus onset asynchronies (SOAs). Neither visual nor acoustic stimuli triggered significant motor responses in nonconditioned animals (Figure S7A; n = 8). However, sound reduced V-CMRs when presented simultaneously or slightly before the flash (SOA = 0 ms, $p < 0.01$; SOA = −25 ms, $p < 0.05$), whereas no effect was observed when sound was presented after the visual stimulus (positive SOAs; Figures 8C and 8D and Figures S7B and S7C; $p > 0.2$). This dependence of the behavioral effect on SOAs is notable, because the latency of visual responses in V1 of awake, freely moving mice (Sawtell et al., 2003) is comparable to the latency of sound-driven responses in V1.

We tested the effects of different sound intensities on hetero-modal behavioral suppression, using the SOA (0 ms; Figure 8D) that gave the largest behavioral suppression. We found no significant acoustic-driven suppression of V-CMRs for the lowest intensity tested (50 dB SPL, $p > 0.2$); however, for higher sound intensities suppression was clearly present and saturated, suggesting an all-or-none effect at behavioral level (Figure 8E; $p < 0.05$ for post hoc tests). Finally, single-trial analysis revealed that heteromodal suppression was due to the combined effect of a reduction in the number of "hits," as well as to a reduction of the amplitude of V-CMRs in the trials where a residual response was still evident (Figure S7D), suggesting degraded processing of the visual stimulus.

To clarify whether the sound-driven suppression of V-CMRs reflected sound-driven inhibition of visual processing in V1, we sought to reduce GABAergic inhibition in V1. Acute intracortical

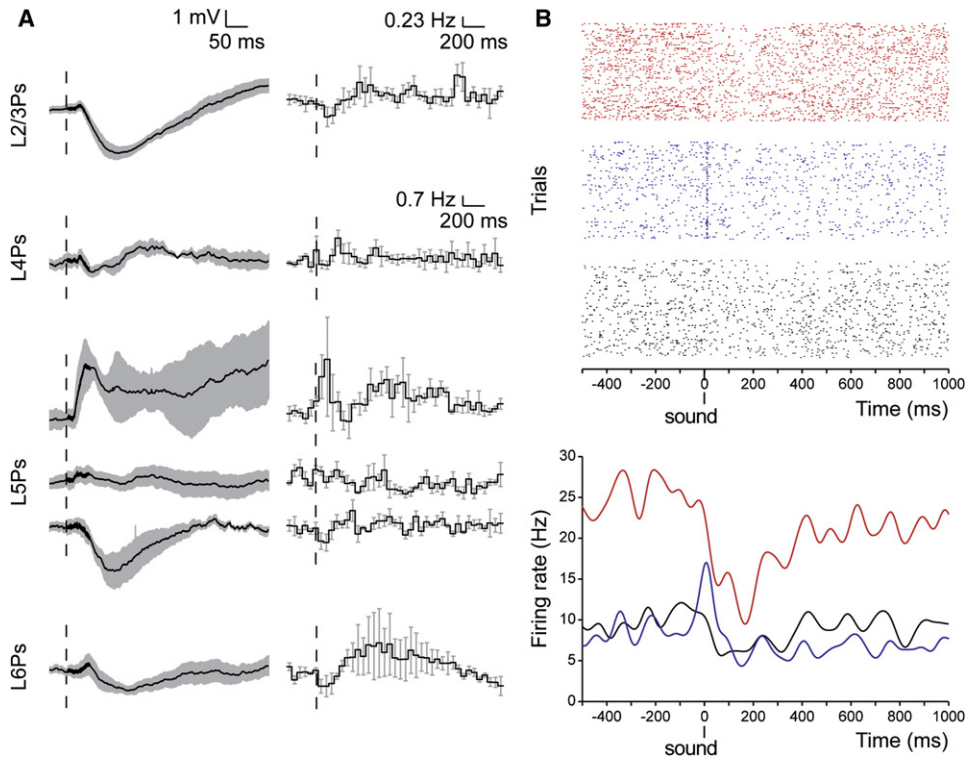

Figure 5. Layer-Specific Effects of Sound on V1 Pyramids

(A) Subthreshold (left) and suprathreshold (right) responses to sound in pyramidal neurons of different layers. Grand averages ± SEM.; bin size: 50 ms. Sound hyperpolarized all L2/3Ps (n = 19) and L6Ps (n = 7). L4Ps were not responsive (n = 5), whereas responses of L5Ps were heterogeneous (from top to bottom: n = 3 depolarizing; n = 5 not responsive; n = 4 hyperpolarizing). Note that the onsets and peaks of depolarizing responses of L5Ps preceded those of SHs in the other layers.

(B) Spike recordings from a tetrode in layer 5 of V1 showing the raster plots (top) and the corresponding instantaneous firing rates (bottom) of three units that were excited, inhibited or unresponsive to noise (blue, red, and black, respectively).

See also Figure S5.

infusion of GABAergic antagonists in V1 (100 μM PTX, 3 μM CGP55845; n = 7; Figure 8F, red) prevented sound-driven inhibition compared to vehicle-injected controls (n = 11, black; $p < 0.01$), demonstrating that behavioral suppression of V-CMRs by sound requires the functional integrity of GABAergic transmission in V1.

DISCUSSION

In this work, we explored how salient stimuli of one sensory modality influence other senses. Through intracellular recordings, we found that activation of a primary sensory cortex (e.g., A1) can inhibit and degrade the performances of neighboring primary sensory cortices (e.g., V1 and somatosensory cortex). In particular, we provide evidence that the activation of A1 by a noise burst elicits hyperpolarizations in the supra- and infragranular layers of V1. This effect is achieved through cortico-cortical inputs that activate an inhibitory subcircuit originating in deep layers of V1.

Transient Heteromodal Stimuli Trigger Widespread Changes in Cortical Network Activity: Role of Inhibition

We found that either noise bursts or optogenetic stimulation of auditory cortex elicited hyperpolarizing responses in nonmatching primary sensory areas. In line with this, focal cortical activations can silence neuronal activity of the neighboring network (Mann et al., 2009; Shu et al., 2003). In vivo, focal photostimulation in monkey neocortex is immediately followed by firing suppression in neighboring units (Han et al., 2009). Moreover, local cortical microstimulation evokes a characteristic EPSP-IPSP sequence (Contreras et al., 1997), mirrored at the suprathreshold level by an early increase in firing followed by a long-lasting suppression (Butovas et al., 2006; Butovas and Schwarz, 2003; Chung and Ferster, 1998). However, AP responses caused by electrical microstimulation in cortex are observed only locally, whereas inhibitory responses can spread for larger distances (Butovas and Schwarz, 2003). The lack of a depolarization before SHs thus suggests that the spread of auditory-driven inhibition might be larger compared to that of excitatory responses. If true, this same mechanism would take place also when other cortical areas, different from A1, are transiently and strongly activated. Indeed, we found that brief multiwhisker stimulation and optogenetic activation of somatosensory and associative cortices elicited hyperpolarizing responses in V1. These results suggest that interareal inhibition is widespread among sensory cortices. However, further experiments will be needed to establish whether somatosensory stimuli and photoactivation of

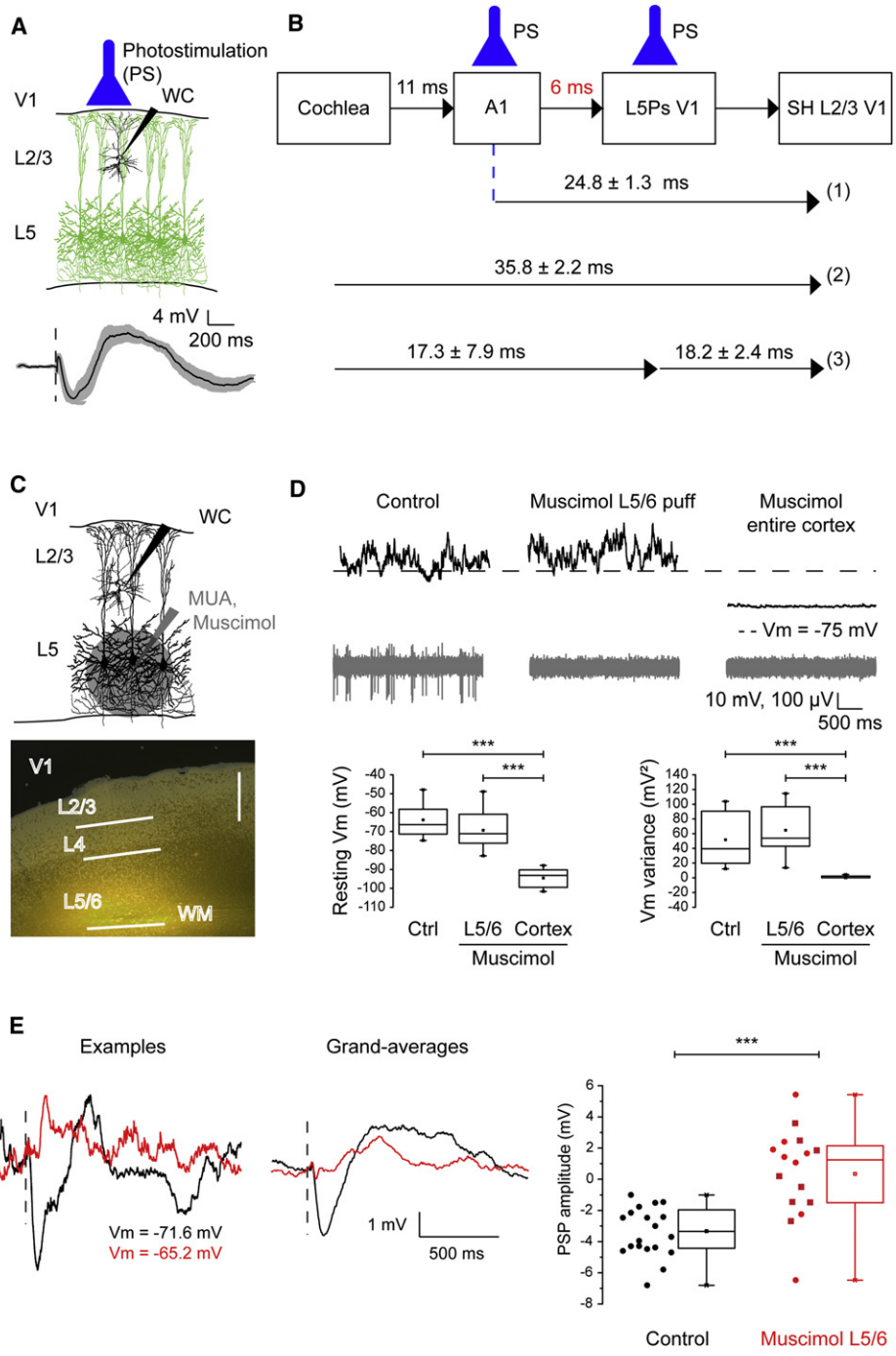

Figure 6. Activation of Infragranular Layers Mediates SHs in L2/3Ps of V1

(A) Photostimulation (PS) of L5Ps hyperpolarized overlying L2/3Ps in V1 (grand-average ± SEM; n = 5).

(B) Diagram showing the mean onset latencies ± SEM of (1) hyperpolarizations of V1 L2/3Ps driven by A1 photostimulation, (2) SHs of L2/3Ps in V1, (3) sound-driven activation of L5Ps in V1 (left) and hyperpolarizations of L2/3Ps in V1 driven by the phostimulation of L5Ps in V1 (right).

(C) Top: whole-cell recordings from L2/3Ps after the injection of muscimol in infragranular layers of V1. Bottom: Nissl-counterstained, coronal section through V1 showing that the injected fluorescent muscimol did not leak into supragranular layers. Bar, 400 µm.

(D) Muscimol abolished spiking in L5 (gray) without modifying the resting V_m of L2/3Ps (black) and its variance over time ("L5/6" in bottom plots). On the contrary, muscimol diffusion to the entire cortex dramatically affected the resting V_m and its variance ("Cortex" in bottom plots, ***$p < 0.001$ for post hoc test).

(E) Acute inactivation of L5/6 activity by a local puff of muscimol counteracted SHs in overlying L2/3Ps of V1 (red, n = 16) with respect to controls (black, n = 19; ***$p < 0.01$). Squares in the box plot (right) indicate the experiments with fluorescent muscimol.

See also Figure S6.

distant sensory areas activate the same inhibitory circuits that are involved in SHs, what happens in intervening areas and which spatial and temporal patterns of activation of a cortical area elicit inter-areal inhibition.

Heteromodal inhibition is reminiscent of up-to-down state transitions occurring during ongoing activity (Figure 1D). In fact, auditory and somatosensory stimuli did not change the spectral content in the frequency band typical of slow cortical oscillations, but simply reset their phase, as in (Kayser et al., 2008). The decrease of membrane resistance during SHs, together with the results of both intracellular and extracellular GABA blockade, indicate that SHs are driven by local, GABAergic synapses. Thus, our data indicate a role for GABA receptor-mediated inhibition in up-to-down-like transitions caused by heteromodal stimuli. This conclusion is in line with the observation that termination of up states induced by electrical stimuli is accompanied by a transient increase of firing of fast spiking interneurons (Shu et al., 2003). Also, $GABA_B$ antagonism prevents electrically induced down states (Mann et al., 2009). In addition, high intracellular chloride (Contreras et al., 1997), as well as $GABA_B$ antagonism (Butovas et al., 2006) prevents long-lasting inhibition evoked in vivo by cortical microstimulation.

Beside the activation of inhibitory inputs, which appear to play a major role in SHs in V1, the analysis of sound-driven changes of synaptic conductances revealed a concurrent, albeit smaller, withdrawal of excitation. The latter may explain the residual hyperpolarization observed in L2/3Ps upon intracellular blockade of GABAergic inputs. Overall, the data support the view that sound-driven activation of GABAergic inputs in the visual cortex trigger a local, transient switch off of the excitatory network.

Possible Interneuronal Subcircuits Underlying SHs in V1

Our findings indicate that heteromodal activation of layer 5 is responsible for SHs of overlying, supragranular pyramids, implying a translaminar inhibitory circuit. Slice works indicate that ascending, back projections from infragranular to supragranular layers are largely inhibitory (Dantzker and Callaway, 2000; Kapfer et al., 2007; Silberberg and Markram, 2007; Xiang et al., 1998; Xu and Callaway, 2009). Importantly, infragranular-to-supragranular inhibition is functionally relevant in vivo, as it shapes both visual (Bolz and Gilbert, 1986) and somatosensory (Murayama et al., 2009) responsiveness.

Which types of interneurons could be responsible for sound-driven translaminar inhibition of L2/3Ps? It seems improbable that fast spiking, parvalbumin-positive cells are the main trigger. Indeed, their activation in vivo drives IPSPs whose fast kinetics is hardly compatible with that of SHs (Cardin et al., 2009). Conversely, at least three types of interneurons are good candidates. Layer 5, somatostatin-positive Martinotti cells receive inputs from neighboring pyramids and send projections to supragranular layers. These projections in turn inhibit neighboring layer 2/3 (Kapfer et al., 2007) and layer 5 pyramids by acting on their apical dendrites (Murayama et al., 2009; Silberberg and Markram, 2007). We found that only a limited number of layer 5 cells are excited by sound, in agreement with a previous extracellular study (Wallace et al., 2004). Since activation of few pyramidal neurons can effectively recruit Martinotti cells (Berger et al., 2010; Kapfer et al., 2007), the possibility exists that the limited number of layer 5 pyramids activated by sound in V1 could activate this form of translaminar inhibition. Notably, synchronous firing of a few pyramidal cells in vivo could effectively trigger inhibition, even with a limited number of spikes (Kapfer et al., 2007). In turn, spiking of few Martinotti cells can generate widespread inhibition on pyramids located in the same, infragranular layers and in supragranular layers (Berger et al., 2010; Kapfer et al.,

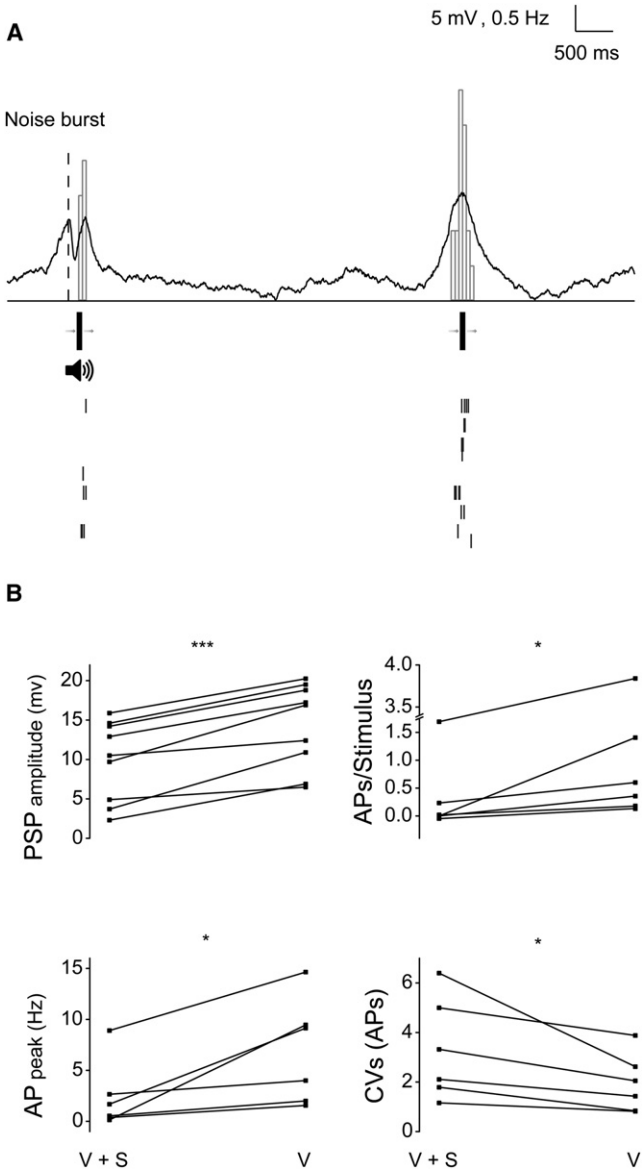

Figure 7. Acoustic Stimulation Reduced Synaptic Responses to Visual Stimuli

(A) Example of averaged sub- and suprathreshold responses (PSTH and raster plot) of a L2/3P in V1 upon stimulation with an optimally oriented moving bar with (left) and without (right) concurrent acoustic stimulation.

(B) Acoustic stimulation reduced subthreshold (top left; ***$p < 0.001$) and suprathreshold (top right and bottom left; *$p < 0.05$) visual responses. Sound also reduced reliability of visually-driven spiking, as expressed by the increase of the coefficient of variation of single-trial AP counts (bottom right; *$p < 0.05$).

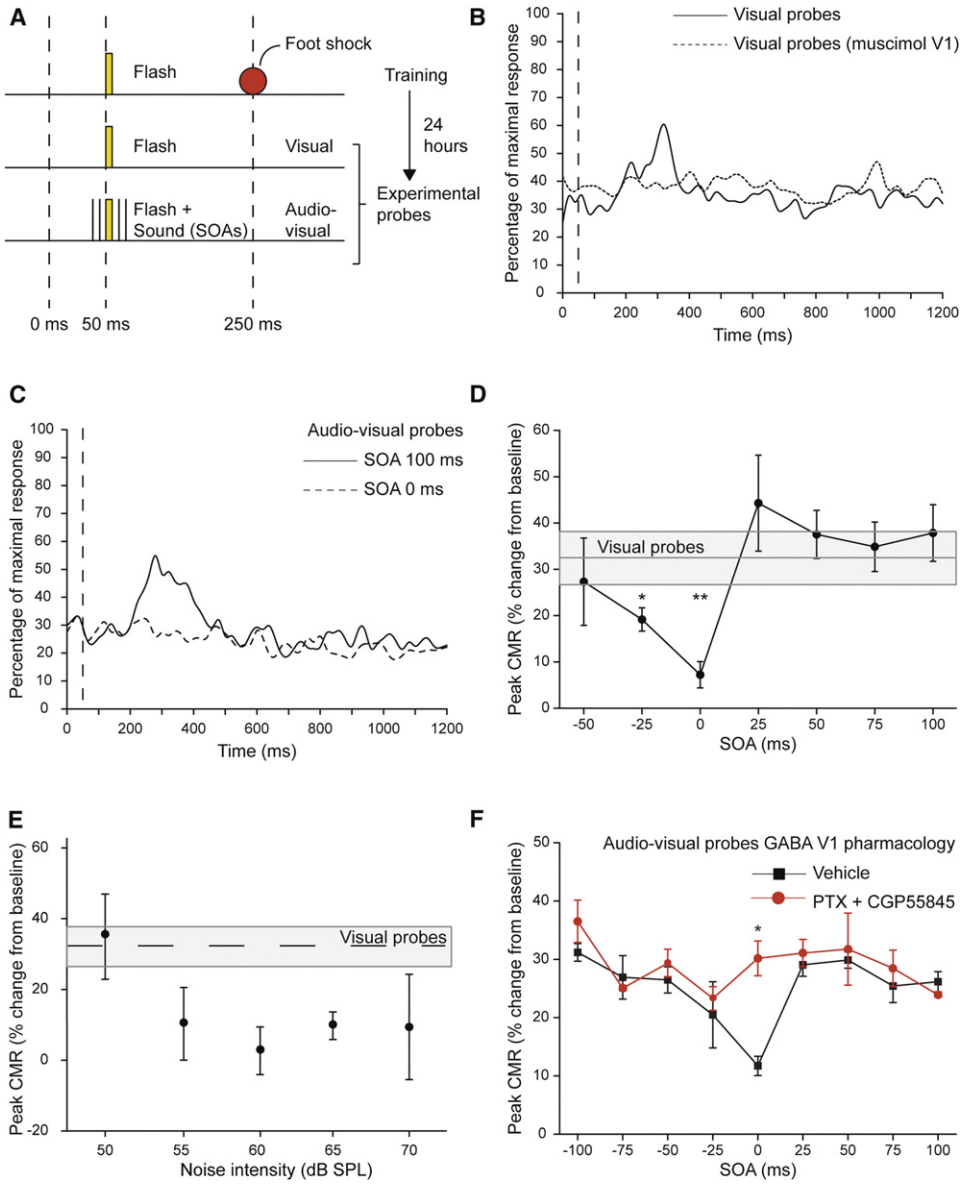

Figure 8. Behavioral Effects of Acoustic Stimulation on a V1-Dependent Task

(A) Protocol to test acoustic influences on visually driven behavior. A flash was paired to a footshock (red), causing the emergence of a V-CMR. Twenty-four hours later, V-CMRs were measured following the pairing of the flash with a noise burst presented at different SOAs.

(B) Time course of the motor activity of the mouse expressed as percentage of the maximal response. Muscimol in V1 (dashed line, n = 8) during conditioning prevented the acquisition of the V-CMR as observed in controls (continuous line, n = 8; $p < 0.01$). Traces represent grand-averages. Vertical dashed line represent flash onset.

(C) Acoustic simulation strongly diminished V-CMRs when presented simultaneously to the flash (SOA 0 ms, dashed line), but not later (SOA +100 ms, continuous line; grand averages are shown, n = 8; $p < 0.01$).

(D) Effect of different SOAs on V-CMRs. Sound significantly reduced V-CMRs when simultaneously presented to light (SOAs = 0 ms and −25 ms; $^{**}p < 0.01$ and $^{*}p < 0.05$, respectively), but not when presented later (SOAs from +25 to +100 ms; $p > 0.2$). Gray bar is the mean V-CMR ± 2SD.

(E) Heteromodal suppression depends on sound intensity. The auditory suppression of V-CMR was present for sound intensities larger than 50 dB SPL and did not depend on sound intensities ($p > 0.3$). Gray bar is mean ± 2SD.

(F) The suppressive effect of sound on V-CMRs was abolished by acute, bilateral infusion of V1 with GABA antagonists (red, 100 μM PTX + 3 μM CGP55845) compared to vehicle-injected controls (black, at SOA 0 ms, $^{*}p < 0.01$ for post hoc test). Means ± SEM are shown.

See also Figure S7.

2007). This possibility is compatible with the presence of SHs in both L2/3Ps and L5Ps, which occurred with comparable onset latencies and kinetics in the two layers (mean onsets: 35.8 versus 37.1 ms, peak latencies: 134.9 versus 104.5 ms for L2/3Ps and L5Ps; see Figure 5A). The delay observed in vitro between L5P firing and the onset of the IPSP mediated by this disynaptic inhibitory circuit onto the target pyramidal neuron (Berger et al., 2010; Kapfer et al., 2007) is in agreement with the delay we observed between the hyperpolarization of L2/3Ps and the excitation of V1 L5Ps, caused by either acoustic or optogenetic stimulation (see Figure 6B). However, our data do not allow establishing whether the laminar position of the activated interneurons is in layers 5/6 and/or 2/3. Indeed, a second possibility is that layer 5 excitatory cells could activate layer 2/3 neurogliaform inhibitory neurons (Xu and Callaway, 2009). Interestingly, a single spike of a neurogliaform cell can elicit long lasting IPSPs mediated by $GABA_A$ and $GABA_B$ receptors on neighboring cortical pyramids (Tamás et al., 2003), causing diffuse network silencing (Oláh et al., 2009). Finally, layer 5 contains also low-threshold spiking interneurons, which send vertically projecting axons to supragranular layers (Xiang et al., 1998). Cell-type-specific inactivation experiments will be required in the near future to dissect among these possibilities.

Anatomical Pathways Underlying Interareal Inhibition

Based on the observed laminar pattern, sound-driven responses in V1 could be generated by horizontal cortico-cortical fibers, nonspecific, associative thalamic systems, or ascending neuromodulatory systems that can activate cortical interneurons (e.g., reviewed in Bacci et al., 2005). Nonspecific thalamic systems receive inputs from layer 5 (Jones, 2001; Theyel et al., 2010), contain multisensory neurons (Avanzini et al., 1980) and send diffuse axonal projections to supragranular layers, irrespective of cortical boundaries (Jones, 2001). Our transection experiments suggest that sound-driven inhibition is relayed to V1 via cortico-cortical connections between auditory and visual cortices, whose existence has been proven in rodents (Campi et al., 2010; Laramée et al., 2011). This finding is in agreement with previous reports indicating that widespread interareal influences, as assessed by multisite FP recordings, rely on cortico-cortical connectivity (Amzica and Steriade, 1995; Frostig et al., 2008). However, we cannot exclude that transections selectively severed thalamo-cortical fibers from higher-order thalamic nuclei, although this seems unlikely. Also, our transection experiments do not allow to distinguish whether the signal is relayed by direct horizontal connections between A1 and V1 or through an intervening cortical area such as V2, which receives auditory inputs (Laramée et al., 2011). However, the estimated brief latency of about 6 ms elapsing between the activation of A1 and the sound-driven activation of L5Ps in V1 is more compatible with a role of direct cortico-cortical connections between A1 and V1. Indeed, a 6 ms latency would be consistent with the propagation speed of sensory evoked cortical activity (0.2–0.5 m/s; Benucci et al., 2007), given the distance between A1 and V1 in mice.

Functional Roles of Interareal Inhibition

Our results indicate that sound-driven IPSPs reduce sub- and suprathreshold responsiveness of visual cortical neurons, resulting in a degradation of visually driven, behavioral responses. Cross-modal, GABAergic inhibition has been described so far in the cat ectosylvian cortex (Dehner et al., 2004). Our results reveal that inter-areal inhibition, far from being restricted to association areas, is already widespread in primary sensory cortices. It could be the synaptic mechanism behind the cross-modal suppressive interactions shown with extracellular recordings in ferrets (Bizley et al., 2007) and macaques (Kayser et al., 2008; Lakatos et al., 2007). Interestingly, cross-modal deactivations have been described also in human occipital cortex using neuroimaging (Laurienti et al., 2002).

Albeit we give evidence that the majority of V1 neurons are inhibited by sound, we also found that this is due to acoustic-driven *excitation* of *few* infragranular cells. This observation is consistent with other reports of spiking responses driven by heteromodal stimuli in primary sensory areas (Bizley et al., 2007; Morrell, 1972; Wallace et al., 2004). In line with our findings, such responses are mostly restricted to deep cortical laminae in rodents (Wallace et al., 2004).

Long-range recruitment of inhibitory subcircuits could be a way to control the fluctuations of subthreshold neural activity in early sensory cortices (Cardin et al., 2009; Traub et al., 1996), and therefore their phase of excitability. In fact, cross-modal modulation of responsiveness in early cortices depends on stimulus onset asynchrony, indicating a time-dependent modulation of cortical excitability induced by heteromodal stimulation (Lakatos et al., 2007). This type of interaction plays a key role in sensory coding, since cross-modal modulation of oscillatory activity in early sensory areas is supposed to add information about external stimuli (Kayser et al., 2010) by providing a time reference to spikes. SHs resetted the phase of ongoing V1 activity and were often followed by a depolarization of the cell. Interestingly, when visual stimuli were presented during the depolarizing plateau, visual responsiveness increased (G.I. and P.M., unpublished data). The GABAergic silencing of local network activity driven by heteromodal stimuli could be the condition allowing the phase-resetting of ongoing activity observed extracellularly by our and other groups (Lakatos et al., 2007).

What is the functional significance of SHs in V1? First, the fact that activation of a primary cortex by a salient stimulus (such as a noise burst in A1) degrades neuronal processing in neighboring areas is in line with the idea that sensory cortices compete for the activation of higher cortical areas. The steep emergence of SHs with increasing sound intensities suggests that, for interareal inhibition to be effective, a certain threshold of activation of A1 has to be reached, particularly to affect the animal's behavior. The fact that SHs were evoked robustly for intensity larger than 55–60 dB SPL is in line with the view that an acoustic stimulus has to be salient for this mechanism to be recruited. Second, it is tempting to speculate that heteromodal inhibition could modulate the selectivity of visual cortical neurons for stimulus attributes such as orientation. The suppressive effects of SHs on visual responsiveness could have a relatively larger impact on responses upon stimuli in the nonpreferred orientation, potentially resulting in a sharpening of orientation tuning. Also, heteromodal GABAergic inhibition may provide a synaptic mechanism subserving divisive gain normalization, an operation that has

been recently proposed to account for important properties of multisensory integration, such as the inverse effectiveness principle and the spatial principle (Ohshiro et al., 2011).

The existence of long-range, competitive interactions between cortical areas and sensory modalities is intriguing given recent models suggesting that inhibitory interactions could play a role in attention (Lee and Maunsell, 2009; Reynolds and Heeger, 2009). In these models, it is posited that the normal mutual inhibitory mechanisms that underlie divisive response-gain normalization in cortex could also subserve the competitive interactions of attention. But attentional interactions are typically examined *within* a cortical area or sensory modality (e.g., visual-visual interactions) and over a relatively small extent of the sensory space (e.g., within a visual hemifield). By analogy, interareal inhibitory interactions could be involved in competitive attentional interactions *between* sensory modalities. On the other hand, we consistently observed a build-up of γ-band activity following heteromodal inhibition in the cortical FP spectra (Figure 1C). The arousing nature of the auditory stimulus used in our experiments could be at the origin of this induction of γ-band activity (Goard and Dan, 2009). This hypothesis predicts an induction of γ-band activity in other areas as well. In this case, coherent gamma-band activity in different primary sensory cortices would allow cross-modal binding of information from different modalities (Senkowski et al., 2008). These will be interesting issues to pursue in more detail in the future.

We did not observe heteromodal hyperpolarizations when we stimulated animals with visual stimuli in nonvisual primary cortices. This indicates that a ''strong'' visual stimulus such as a flash or a low spatial frequency pattern cannot evoke detectable interareal inhibition. The observed asymmetry could reflect the relative importance of the different senses in rodents, which rely less on visual stimuli compared to more visual carnivores and primates. In line with the existence of species-specific differences of intermodal effects, is also the literature showing the existence of visual influences, in particular in the auditory cortex of higher mammals, that we could not replicate in mice. The lack of visual influences on the auditory cortices could be due to the fact that we limited our intracellular recordings to the supragranular layers. However, extracellular multiunit recordings in deeper layers (granular and infragranular) confirmed the lack of detectable visually driven spike responses in these deeper laminae (Figure S3D). Still, the possibility remains that subthreshold visual inputs—that cannot be directly revealed by extracellular recordings—impinge onto deeper auditory neurons, in line with the existence of anatomo-functional contacts between the secondary visual cortex and auditory cortex (Banks et al., 2011).

In conclusion, we show that the interplay between different senses can occur by means of interareal synaptic inhibition. The elucidation of the synaptic basis of multimodal interactions in primary sensory areas could pave the way for further exploration of how a complete sensory deprivation of one modality during development affects interareal connectivity and the local microcircuitry (Bavelier and Neville, 2002). Intriguingly, such sensory deprivations cause anatomically detectable changes of the GABAergic system in the affected primary cortices (Sanchez-Vives et al., 2006).

EXPERIMENTAL PROCEDURES

Surgery and Anesthesia

Four to six weeks C57BL/6J mice were used throughout all experiments adhering to the Italian Health Ministry Guidelines and Permissions. Mice were lightly anaesthetized under urethane (ca 0.9 g/kg i.p.) and anesthesia depth was monitored using FPs and membrane potential spectra, together with physiological signs. Recordings in awake, head-fixed mice were done after implantation of a recording chamber and habituation to the setup. Craniotomies in V1, A1, and S1 were guided by ISI through the thinned skull. Injections of muscimol (both normal and fluorescent) in A1 and in V1 were done with a pressure-injection device (Picospritzer, General Valve, UK). Transections were done rostrocaudally based on ISI of V1 and A1 and were done with a 30 gauge blade: the depth and coronal height of the transection were verified postmortem in Nissl-counterstained sections. Cannulae for acute pharmacology were implanted in the center of V1 5–6 days before experiments (done within 10–15 min from infusion of 0.7 μl of drugs).

Electrophysiology and Histology

Single-, multiunit, and FP recordings were done using 1–3 MΩ borosilicate or tungsten electrodes for acute or chronic recordings in freely moving animals, respectively. In vivo whole-cell recordings were done in current clamp using an EPC 10 double-plus amplifier (HEKA, Germany) using 5–9 MΩ borosilicate pipettes. Series resistance, spike height and resting Vm were stable throughout recordings (duration: 15–120 min). No holding currents were used unless for excitatory and inhibitory conductances estimates. At the end of the experiments, animals were perfused with fixative and biocytin-filled cells were revealed together with layering for cell recovery.

Analysis of Intracellular Responses

For PSP measurements, sweeps have been averaged after spike removal, whereas for AP counts, 50 ms binning was applied. Unless otherwise stated, PSP amplitudes have been measured in the 0–300 ms poststimulus time window, whereas onset latencies were taken when the V_m was larger than 2 standard deviations above baseline. For conductance measurements and extracellular data analysis, see Supplemental Experimental Procedures.

Sensory and Optogenetic Stimulations

Stimuli were delivered every 5–7 s and were: broad band noise bursts (50 ms, 72 dB SPL; ambient noise level: 35 dB SPL); 20 × 20 deg spots flashed in the upper central visual field, 0.05 C/deg gratings alternating in counterphase, or, in the case of bimodal stimulation, optimally oriented 3 deg wide bars; piezoelectrically driven 10 deg whiskers displacements. In the latter case, ears were plugged and eyes closed. Photostimulation in Thy1::ChR2-EYFP mice was done by coupling a 473 nm laser to an optic fiber (NA 0.22, 20 mW/mm2) and delivering 1ms pulse every 5 s.

Behavior

Mice were first conditioned by 20 parings of flashes with footshocks. Twenty-four hours later, V-CMRs and the effects of sound presentations at different SOAs over them were measured using an accelerometer (TSE systems, Germany).

Statistical Methods

For normally distributed data means ± SEM. are reported, otherwise medians are reported. Normally distributed data were compared using either paired or unpaired Student's t tests, whereas nonnormally distributed data were compared with Mann-Whitney U statistic. Multiple comparisons were done by one-way ANOVA followed by Tukey post hoc test for normally distributed data, or by one-way ANOVA on ranks followed by Dunn post hoc test for nonnormally distributed data. For the acute pharmacology in behaving mice, two-way ANOVA followed by Fisher post hoc tests were used. Full details in Supplemental Material.

SUPPLEMENTAL INFORMATION

Supplemental Information includes seven figures and supplemental text and can be found with this article online at doi:10.1016/j.neuron.2011.12.026.

ACKNOWLEDGMENTS

We thank Drs. Tommaso Pizzorusso, Matteo Caleo, and Prof. John Assad for critically reading the manuscript and Dr. Giacomo Pruzzo and Dr Alessandro Parodi for technical assistance. Grant support was from ISS Young Researchers (to P.M.), Compagnia di San Paolo of Torino (to P.M. and F.B.), Telethon Italy Grant GGP09134 (to F.B.).

Accepted: December 9, 2011
Published: February 22, 2012

REFERENCES

Amzica, F., and Steriade, M. (1995). Disconnection of intracortical synaptic linkages disrupts synchronization of a slow oscillation. J. Neurosci. *15*, 4658–4677.

Avanzini, G., Broggi, G., Franceschetti, S., and Spreafico, R. (1980). Multisensory convergence and interaction in the pulvinar-lateralis posterior complex of the cat's thalamus. Neurosci. Lett. *19*, 27–32.

Bacci, A., Huguenard, J.R., and Prince, D.A. (2005). Modulation of neocortical interneurons: extrinsic influences and exercises in self-control. Trends Neurosci. *28*, 602–610.

Banks, M.I., Uhlrich, D.J., Smith, P.H., Krause, B.M., and Manning, K.A. (2011). Descending projections from extrastriate visual cortex modulate responses of cells in primary auditory cortex. Cereb. Cortex *21*, 2620–2638.

Bavelier, D., and Neville, H.J. (2002). Cross-modal plasticity: where and how? Nat. Rev. Neurosci. *3*, 443–452.

Benucci, A., Frazor, R.A., and Carandini, M. (2007). Standing waves and traveling waves distinguish two circuits in visual cortex. Neuron *55*, 103–117.

Berger, T.K., Silberberg, G., Perin, R., and Markram, H. (2010). Brief bursts self-inhibit and correlate the pyramidal network. PLoS Biol. *8*, 8.

Bizley, J.K., Nodal, F.R., Bajo, V.M., Nelken, I., and King, A.J. (2007). Physiological and anatomical evidence for multisensory interactions in auditory cortex. Cereb. Cortex *17*, 2172–2189.

Bolz, J., and Gilbert, C.D. (1986). Generation of end-inhibition in the visual cortex via interlaminar connections. Nature *320*, 362–365.

Butovas, S., and Schwarz, C. (2003). Spatiotemporal effects of microstimulation in rat neocortex: a parametric study using multielectrode recordings. J. Neurophysiol. *90*, 3024–3039.

Butovas, S., Hormuzdi, S.G., Monyer, H., and Schwarz, C. (2006). Effects of electrically coupled inhibitory networks on local neuronal responses to intracortical microstimulation. J. Neurophysiol. *96*, 1227–1236.

Campi, K.L., Bales, K.L., Grunewald, R., and Krubitzer, L. (2010). Connections of auditory and visual cortex in the prairie vole (Microtus ochrogaster): evidence for multisensory processing in primary sensory areas. Cereb. Cortex *20*, 89–108.

Cardin, J.A., Carlén, M., Meletis, K., Knoblich, U., Zhang, F., Deisseroth, K., Tsai, L.H., and Moore, C.I. (2009). Driving fast-spiking cells induces gamma rhythm and controls sensory responses. Nature *459*, 663–667.

Chung, S., and Ferster, D. (1998). Strength and orientation tuning of the thalamic input to simple cells revealed by electrically evoked cortical suppression. Neuron *20*, 1177–1189.

Contreras, D., Dürmüller, N., and Steriade, M. (1997). Absence of a prevalent laminar distribution of IPSPs in association cortical neurons of cat. J. Neurophysiol. *78*, 2742–2753.

Crochet, S., and Petersen, C.C. (2006). Correlating whisker behavior with membrane potential in barrel cortex of awake mice. Nat. Neurosci. *9*, 608–610.

Dantzker, J.L., and Callaway, E.M. (2000). Laminar sources of synaptic input to cortical inhibitory interneurons and pyramidal neurons. Nat. Neurosci. *3*, 701–707.

DeFelipe, J., Conley, M., and Jones, E.G. (1986). Long-range focal collateralization of axons arising from corticocortical cells in monkey sensory-motor cortex. J. Neurosci. *6*, 3749–3766.

Dehner, L.R., Keniston, L.P., Clemo, H.R., and Meredith, M.A. (2004). Cross-modal circuitry between auditory and somatosensory areas of the cat anterior ectosylvian sulcal cortex: a 'new' inhibitory form of multisensory convergence. Cereb. Cortex *14*, 387–403.

Douglas, R.J., and Martin, K.A. (1991). A functional microcircuit for cat visual cortex. J. Physiol. *440*, 735–769.

Driver, J., and Noesselt, T. (2008). Multisensory interplay reveals crossmodal influences on 'sensory-specific' brain regions, neural responses, and judgments. Neuron *57*, 11–23.

Fishman, M.C., and Michael, P. (1973). Integration of auditory information in the cat's visual cortex. Vision Res. *13*, 1415–1419.

Fontanini, A., and Katz, D.B. (2006). State-dependent modulation of time-varying gustatory responses. J. Neurophysiol. *96*, 3183–3193.

Frostig, R.D., Xiong, Y., Chen-Bee, C.H., Kvasnák, E., and Stehberg, J. (2008). Large-scale organization of rat sensorimotor cortex based on a motif of large activation spreads. J. Neurosci. *28*, 13274–13284.

Ghazanfar, A.A., Maier, J.X., Hoffman, K.L., and Logothetis, N.K. (2005). Multisensory integration of dynamic faces and voices in rhesus monkey auditory cortex. J. Neurosci. *25*, 5004–5012.

Goard, M., and Dan, Y. (2009). Basal forebrain activation enhances cortical coding of natural scenes. Nat. Neurosci. *12*, 1444–1449.

Gradinaru, V., Mogri, M., Thompson, K.R., Henderson, J.M., and Deisseroth, K. (2009). Optical deconstruction of parkinsonian neural circuitry. Science *324*, 354–359.

Han, X., Qian, X., Bernstein, J.G., Zhou, H.H., Franzesi, G.T., Stern, P., Bronson, R.T., Graybiel, A.M., Desimone, R., and Boyden, E.S. (2009). Millisecond-timescale optical control of neural dynamics in the nonhuman primate brain. Neuron *62*, 191–198.

Higley, M.J., and Contreras, D. (2005). Integration of synaptic responses to neighboring whiskers in rat barrel cortex in vivo. J. Neurophysiol. *93*, 1920–1934.

Jones, E.G. (2001). The thalamic matrix and thalamocortical synchrony. Trends Neurosci. *24*, 595–601.

Kapfer, C., Glickfeld, L.L., Atallah, B.V., and Scanziani, M. (2007). Supralinear increase of recurrent inhibition during sparse activity in the somatosensory cortex. Nat. Neurosci. *10*, 743–753.

Kayser, C., Petkov, C.I., and Logothetis, N.K. (2008). Visual modulation of neurons in auditory cortex. Cereb. Cortex *18*, 1560–1574.

Kayser, C., Logothetis, N.K., and Panzeri, S. (2010). Visual enhancement of the information representation in auditory cortex. Curr. Biol. *20*, 19–24.

Lakatos, P., Chen, C.M., O'Connell, M.N., Mills, A., and Schroeder, C.E. (2007). Neuronal oscillations and multisensory interaction in primary auditory cortex. Neuron *53*, 279–292.

Lakatos, P., Karmos, G., Mehta, A.D., Ulbert, I., and Schroeder, C.E. (2008). Entrainment of neuronal oscillations as a mechanism of attentional selection. Science *320*, 110–113.

Laramée, M.E., Kurotani, T., Rockland, K.S., Bronchti, G., and Boire, D. (2011). Indirect pathway between the primary auditory and visual cortices through layer V pyramidal neurons in V2L in mouse and the effects of bilateral enucleation. Eur. J. Neurosci. *34*, 65–78.

Laurienti, P.J., Burdette, J.H., Wallace, M.T., Yen, Y.F., Field, A.S., and Stein, B.E. (2002). Deactivation of sensory-specific cortex by cross-modal stimuli. J. Cogn. Neurosci. *14*, 420–429.

Lee, J., and Maunsell, J.H. (2009). A normalization model of attentional modulation of single unit responses. PLoS ONE *4*, e4651.

Mann, E.O., Kohl, M.M., and Paulsen, O. (2009). Distinct roles of GABA(A) and GABA(B) receptors in balancing and terminating persistent cortical activity. J. Neurosci. *29*, 7513–7518.

Morrell, F. (1972). Visual system's view of acoustic space. Nature *238*, 44–46.

Murayama, M., Pérez-Garci, E., Nevian, T., Bock, T., Senn, W., and Larkum, M.E. (2009). Dendritic encoding of sensory stimuli controlled by deep cortical interneurons. Nature *457*, 1137–1141.

Niell, C.M., and Stryker, M.P. (2010). Modulation of visual responses by behavioral state in mouse visual cortex. Neuron *65*, 472–479.

Ohshiro, T., Angelaki, D.E., and DeAngelis, G.C. (2011). A normalization model of multisensory integration. Nat. Neurosci. *14*, 775–782.

Oláh, S., Füle, M., Komlósi, G., Varga, C., Báldi, R., Barzó, P., and Tamás, G. (2009). Regulation of cortical microcircuits by unitary GABA-mediated volume transmission. Nature *461*, 1278–1281.

Otazu, G.H., Tai, L.H., Yang, Y., and Zador, A.M. (2009). Engaging in an auditory task suppresses responses in auditory cortex. Nat. Neurosci. *12*, 646–654.

Paperna, T., and Malach, R. (1991). Patterns of sensory intermodality relationships in the cerebral cortex of the rat. J. Comp. Neurol. *308*, 432–456.

Petersen, C.C., Hahn, T.T., Mehta, M., Grinvald, A., and Sakmann, B. (2003). Interaction of sensory responses with spontaneous depolarization in layer 2/3 barrel cortex. Proc. Natl. Acad. Sci. USA *100*, 13638–13643.

Reynolds, J.H., and Heeger, D.J. (2009). The normalization model of attention. Neuron *61*, 168–185.

Sakata, S., and Harris, K.D. (2009). Laminar structure of spontaneous and sensory-evoked population activity in auditory cortex. Neuron *64*, 404–418.

Sanchez-Vives, M.V., Nowak, L.G., Descalzo, V.F., Garcia-Velasco, J.V., Gallego, R., and Berbel, P. (2006). Crossmodal audio-visual interactions in the primary visual cortex of the visually deprived cat: a physiological and anatomical study. Prog. Brain Res. *155*, 287–311.

Sawtell, N.B., Frenkel, M.Y., Philpot, B.D., Nakazawa, K., Tonegawa, S., and Bear, M.F. (2003). NMDA receptor-dependent ocular dominance plasticity in adult visual cortex. Neuron *38*, 977–985.

Senkowski, D., Schneider, T.R., Foxe, J.J., and Engel, A.K. (2008). Crossmodal binding through neural coherence: implications for multisensory processing. Trends Neurosci. *31*, 401–409.

Shu, Y., Hasenstaub, A., and McCormick, D.A. (2003). Turning on and off recurrent balanced cortical activity. Nature *423*, 288–293.

Shuler, M.G., and Bear, M.F. (2006). Reward timing in the primary visual cortex. Science *311*, 1606–1609.

Silberberg, G., and Markram, H. (2007). Disynaptic inhibition between neocortical pyramidal cells mediated by Martinotti cells. Neuron *53*, 735–746.

Stein, B.E., and Stanford, T.R. (2008). Multisensory integration: current issues from the perspective of the single neuron. Nat. Rev. Neurosci. *9*, 255–266.

Tamás, G., Lorincz, A., Simon, A., and Szabadics, J. (2003). Identified sources and targets of slow inhibition in the neocortex. Science *299*, 1902–1905.

Theyel, B.B., Llano, D.A., and Sherman, S.M. (2010). The corticothalamocortical circuit drives higher-order cortex in the mouse. Nat. Neurosci. *13*, 84–88.

Traub, R.D., Whittington, M.A., Stanford, I.M., and Jefferys, J.G. (1996). A mechanism for generation of long-range synchronous fast oscillations in the cortex. Nature *383*, 621–624.

Tsodyks, M., Kenet, T., Grinvald, A., and Arieli, A. (1999). Linking spontaneous activity of single cortical neurons and the underlying functional architecture. Science *286*, 1943–1946.

Wallace, M.T., Ramachandran, R., and Stein, B.E. (2004). A revised view of sensory cortical parcellation. Proc. Natl. Acad. Sci. USA *101*, 2167–2172.

Xiang, Z., Huguenard, J.R., and Prince, D.A. (1998). Cholinergic switching within neocortical inhibitory networks. Science *281*, 985–988.

Xu, X., and Callaway, E.M. (2009). Laminar specificity of functional input to distinct types of inhibitory cortical neurons. J. Neurosci. *29*, 70–85.